Biophysical studies on interactions and assembly of full-size E3 ubiquitin ligase : suppressor of cytokine signaling 2 (SOCS2)-elongin BC-cullin 5-ring box protein 2 (RBX2)

THE JOURNAL OF BIOLOGICAL CHEMISTRY VOL.XXX, NO.XX, pp. XXXX-XXXX, 2014

Biophysical studies on interactions and assembly of full-size E3 ubiquitin ligase SOCS2-EloBC-Cul5-Rbx2

Emil Bulatov[‡§], Esther M. Martin[¶], Sneha Chatterjee[¶], Axel Knebel[§], Satoko Shimamura[#], Albert Konijnenberg[¶], Clare Johnson[§], Nico Zinn[#], Paola Grandi[#], Frank Sobott[¶] and Alessio Ciulli[‡§1]

From the [‡]Department of Chemistry, University of Cambridge, Cambridge, CB2 1EW, UK, the [§]College of Life Sciences, University of Dundee, Dundee, DD1 5EH, UK, the [#]Cellzome GmbH, Meyerhofstrasse 1, 69117 Heidelberg, Germany, the [¶]Department of Chemistry, University of Antwerp, 2020 Antwerpen, Belgium.

Running title: Assembly and Interactions of $CRL5^{SOCS2}$ E3 ligase

[1]To whom correspondence should be addressed: Dr. Alessio Ciulli, College of Life Sciences, University of Dundee, Dow Street, Dundee, DD15EH, UK. Tel.: +44(0)1382-386230; E-mail: a.ciulli@dundee.ac.uk

Keywords: ubiquitin ligase, protein-protein interaction, protein complex, protein assembly, biophysics, Cullin

Background: The component subunits of CRL E3 ligases such as substrate receptor, adaptor, Cullin scaffold and RING domain protein assemble into full-size complexes.
Results: Components of $CRL5^{SOCS2}$ were identified from human cell lysate, the full-size complex was reconstituted *in vitro* using recombinant proteins and protein-protein interactions were biophysically characterized.
Conclusion: $CRL5^{SOCS2}$ exists in a monomeric state and the proposed structural model is supported by native ion-mobility electrospray mass spectrometry.
Significance: The results provide structural insights into assembly of the full-size $CRL5^{SOCS2}$ and can aid the development of small molecules targeting the CRL complexes.

ABSTRACT

The multi-subunit Cullin RING E3 ubiquitin ligases (CRLs) target post-translationally modified substrates for ubiquitination and proteasomal degradation. The suppressors of cytokine signaling (SOCS) proteins play important roles in inflammatory processes, diabetes and cancer, and therefore represent attractive targets for therapeutic intervention. The SOCS proteins, amongst their other functions, serve as substrate receptors of CRL5 complexes. A member of the CRL family, SOCS2-EloBC-Cul5-Rbx2 ($CRL5^{SOCS2}$) binds phosphorylated growth hormone receptor (GHR) as its main substrate. Here, we demonstrate that the components of $CRL5^{SOCS2}$ can be specifically pulled from K562 human cell lysates using beads decorated with phosphorylated GHR peptides. Subsequently, SOCS2-EloBC and full-length Cul5-Rbx2, recombinantly expressed in *E. coli* and in Sf21 insect cells, respectively, were used to reconstitute $CRL5^{SOCS2}$ complexes *in vitro*. Finally, diverse biophysical methods were employed to study the assembly and interactions within the complexes. Unlike many other E3 ligases, the $CRL5^{SOCS2}$ was found to exist in a monomeric state as confirmed by size exclusion chromatography with inline multi-angle static light scattering (SEC-MALS) and native mass spectrometry (MS). Affinities of the protein-protein interactions within the multi-subunit complex were measured by isothermal titration calorimetry (ITC). A structural model for the full-size $CRL5^{SOCS2}$ is supported by travelling wave ion-mobility mass spectrometry (TWIM-MS) data.

Cullin RING E3 ubiquitin ligases (CRLs) represent the largest known family of E3 enzymes in the ubiquitin-proteasome system (>200 CRLs out of total >600 E3 enzymes) and play a significant role in cancer and other diseases (1). In some types of cells up to 20% of the proteasome-dependent degradation is mediated by CRLs (2). Assembly of the multi-subunit CRLs was initially reported for the archetypal Skp1-Cul1-Rbx1 complex (3). CRLs use modular subunit organization consisting of interchangeable adaptors (Skp1, ElonginB, ElonginC, DDB1, BTB), substrate receptors (F-box, SOCS-box, DCAF, BTB), Cullin scaffolds (Cullin1-7) and RING domain proteins (Rbx1 and Rbx2) to enable assembly of a large number of functionally diverse E3 ligase complexes (1, 4, 5).

The N-terminal domain (NTD) of Cullin proteins consists of three five-helix bundles ("cullin repeats") that form a long-stalk architecture, and a globular C-terminal domain (CTD, or "cullin homology domain"). Cullin NTD recruits variable substrate receptors either directly or via an adaptor protein, whereas Cullin CTD serves as a docking site for RING domain proteins that in turn recruits a cognate ubiquitin-loaded E2 (6). RING domain proteins contain a distinct Zn^{2+}-binding domain characterized by a canonical RING motif. Selection of the substrate receptors for a particular CRL occurs through a specific receptor LPXP motif that forms a minor yet crucial supplementary interaction with Cullin NTD (7, 8).

SOCS2 is a member of the SOCS-box protein family that in association with the adaptor ElonginB-ElonginC complex (EloBC), Cullin5 scaffold and Rbx2 constitutes a $CRL5^{SOCS2}$ E3 ligase. SOCS2 contains three structural domains: a conserved C-terminal SOCS-box domain that binds to adaptor EloBC; a central SH2 domain mediating recruitment of phosphorylated tyrosine-containing sequence of the substrate; and a variable N-terminal region that facilitates interaction with the substrate. $CRL5^{SOCS2}$ negatively regulates growth hormone signaling by targeting growth hormone receptor (GHR) for ubiquitination and proteasomal degradation (9). Phosphorylated tyrosine pY595 serves as the key structural determinant of GHR recognition by the SH2 domain of SOCS2 (10). Crystal structures of SOCS2-EloBC (PDB 2C9W) (11) and SOCS2-EloBC-$Cul5_{NTD}$ (PDB 4JGH) (12) describe structural features of the protein-protein interfaces within these left-arm complexes. However, the details of assembly of the full-size $CRL5^{SOCS2}$ E3 complex both *in vivo* and *in vitro* remain missing.

In recent years interest in studying structure, function and assembly of CRLs has been growing, notably driven in part by their potential role as drug targets in a number of human diseases (13-16). Yet, only a few studies have investigated the full-size CRL complexes biophysically, primarily due to difficulties in obtaining some of the protein components recombinantly, in particular full-length Cullins. Furthermore, large heteromeric protein complexes such as CRLs are notoriously tough to crystallize into diffraction-quality crystals. Therefore, it seems promising to engage the strengths of diverse biophysical methods in order to facilitate characterization of both the individual subunits and the full-size complexes as well as provide means for examining their association and interactions.

Here, we show that all components of the $CRL5^{SOCS2}$ can be pulled down from a cell lysate via SOCS2-mediated recognition of the phosphorylated GHR_pY595 peptide immobilised on beads. The full-length E3 ligase complex is then reconstituted *in vitro* using purified recombinant proteins and characterized biophysically. Investigations of assembly and interactions within the complex are carried out using size exclusion chromatography and multi-angle light scattering (SEC-MALS), isothermal titration calorimetry (ITC) and nanoelectrospray travelling wave-ion mobility mass spectrometry (TWIM-MS).

EXPERIMENTAL PROCEDURES

Pull-down experiments – Pull-down experiments were performed using biotinylated GHR-derived 11-mer peptides phosphorylated (GHR_pY595) or not (GHR_Y595) on tyrosine 595, harbouring aminohexanoic acid (ahx) as spacer after the biotin (Biotin-ahx-PVPDpYTSIHIV-amide) and immobilized on high capacity Neutravidin beads. Competition experiments were performed by incubating human K562 total cell lysate with 100 µM of non-biotinylated phosphorylated peptide (GHR_pY595) and the immobilized (Biotin-ahx-

PVPDpYTSIHIV-amide) beads for 2 hours at 4°C. After washing, bound proteins were eluted with SDS-sample buffer and prepared for Tandem Mass Tags (TMT) labeling and MS analysis as described in (17)

Protein expression and purification – Recombinant human SOCS2 (amino acids 32–198), ElonginC (17–112), and ElonginB (1-118) were co-expressed in *E. coli* BL21(DE3) from the pLIC (SOCS2) and pCDF_Duet (EloBC) plasmids (gifts from A. Bullock, SGC Oxford, UK). A starter culture was grown overnight from a single transformant colony using 50 mL of LB media containing 100 μg/mL ampicillin and 50 μg/mL streptomycin. Starter culture then was used to inoculate 7 L of LB media containing 100 μg/mL ampicillin and 50 μg/mL streptomycin. The cells were grown at 37°C until OD_{600} ~0.7, cooled to 18°C, then protein expression was induced with 1mM IPTG for 12 hours.

Recombinant human $Cul5_{NTD}$ (N-terminal domain, 1-386) was expressed in *E. coli* BL21(DE3) from a pNIC plasmid encoding sequence for $Cul5_{NTD}$, containing His_6 and FLAG tags at the C-terminal end and a Tobacco Etch Virus (TEV) cleavage site, as previously described (18). Briefly, 50 mL of starter culture was grown overnight using a single transformant colony in LB media containing 50 μg/mL kanamycin and used to inoculate 2 L LB media supplemented with 50 μg/mL kanamycin. The cells were grown at 37°C until OD_{600} ~0.7, cooled to 18°C and protein expression was induced with 0.5mM IPTG for 12 hours.

Recombinant SOCS2-EloBC and $Cul5_{NTD}$ were independently purified using the following protocol. The cell pellets were harvested by centrifugation at 5000 rpm, 4°C for 30 min and resuspended in Binding buffer (50mM HEPES pH 7.5, 500 mM NaCl, 5% glycerol, 0.5 mM TCEP). The supernatant was treated with 10 μg/mL DNAse I, 10 mM $MgCl_2$ for 30 min and then filtered through a 0.22 μm filter. The sample was applied on a HisTrap column (GE Healthcare), the resin washed with Wash buffer (50mM HEPES pH 7.5, 20 mM Imidazole, 500 mM NaCl, 5% glycerol, 0.5 mM TCEP) and then eluted with the incremental gradient of Elution buffer (50mM HEPES pH 7.5, 500 mM Imidazole, 500 mM NaCl, 5% glycerol, 0.5 mM TCEP). Fractions containing protein were pooled and the His_6-tag was cleaved off by overnight dialysis in the presence of TEV protease at 4°C in Binding buffer. The protein was applied to a HisTrap column for a second time, collecting the flow-through, then concentrated and purified on a HiLoad 16/60 Superdex 75 column with running buffer 25 mM HEPES pH=7.5, 250 mM NaCl, 0.5 mM TCEP.

Recombinant human Cul5 (amino acids 1-780) and Rbx2 (amino acids 1-113) were co-expressed in Sf21 insect cells using pFastBac™ Dual vector in Bac-to-Bac® baculovirus expression system. In this vector Cul5 is N-terminally tagged with a fragment of bacterial PBP5 (Dac-tag) (19), which can be removed with TEV protease, as previously described (20).

Bacmids for Dac-TEV-Cul5/Rbx2 were generated in DH10BAC cells and transfected into Sf21 cells, using Cellfectin II ® (Invitrogen). The transfected cells were kept for 7 days at 27ºC in Insect Express® medium (Lonza), supplemented with ANTI-ANTI® (Invitrogen). The cells were sedimented and the virus containing supernatant was used to infect 150 ml of Sf21 culture at a density of 1.5 x 10^6 cells / ml. For the expression of RING E3 ligases we supplement the Insect Express medium with 5 μM $ZnCl_2$. After 5 days the cells were collected under sterile conditions and the supernatant was used to infect 2L of Sf21 cell culture for 3 days. The Cul5-Rbx2 protein complex was purified using the following procedure. Cells were harvested by centrifugation at 3500 rpm, 4°C for 15 min, then resuspended in 25 mL of 50 mM HEPES pH 7.4, 0.1 mM EGTA, 1 μM $ZnCl_2$, 1 mM TCEP, 1mM Pefabloc® and 20μg/ml Leupeptin (both from Apollo Scientific) and incubated for 15 min at 4°C. Cells were sheared using a 50 ml tight fit Dounce homogenizer and insoluble material was removed by centrifugation at 40000 rpm, 10°C for 20 min. To perform Dac-affinity purification the supernatant was gently mixed with ampicillin-Sepharose at room temperature for 50 min. The Sepharose was collected by centrifugation and washed 6 times in 10 volumes of 50 mM HEPES pH 7.4, 150 mM NaCl, 0.1 mM EGTA, 1 μM $ZnCl_2$, 1 mM TCEP. To recover untagged Cul5-Rbx2, the Sepharose was incubated with TEV protease (50μg TEV / 1ml Sepharose) overnight at

room temperature and drained and washed through Econopac® filter units (Bio-Rad). The Cul5-Rbx2 protein was concentrated and further purified by preparative size-exclusion chromatography using HiLoad 16/600 Superdex 200 column (GE Healthcare) with 50 mM HEPES pH 7.4, 150 mM NaCl, 10% glycerol, 0.5 mM TCEP.

The identity and purity of all obtained proteins was confirmed using denaturing ESI-MS and SDS-PAGE. All proteins were flash frozen using liquid nitrogen and stored at -80 °C.

Reconstitution of SOCS2-EloBC-Cul5$_{NTD}$ and SOCS2-EloBC-Cul5-Rbx2 protein complexes – To form quaternary SOCS2-EloBC-Cul5$_{NTD}$ complex, Cul5$_{NTD}$ and SOCS2-EloBC were mixed together at a 1:1.1 molar ratio and incubated at room temperature for 30 min, following purification of the complex using a HiLoad 16/600 Superdex 75 column in 25 mM HEPES pH 7.5, 250 mM NaCl, 0.5 mM TCEP.

To form the pentameric complex, Cul5-Rbx2 and SOCS2-EloBC were mixed at a 1:1.1 molar ratio and incubated at room temperature for 30 min. The protein complex was purified using HiLoad 16/600 Superdex 200 column in 50 mM HEPES pH 7.4, 150 mM NaCl, 10% glycerol, 0.5 mM TCEP. SDS-PAGE analysis of SOCS2-EloBC, Cul5$_{NTD}$, SOCS2-EloBC-Cul5$_{NTD}$, Cul5-Rbx2 and SOCS2-EloBC-Cul5-Rbx2 are shown in Figure S2.

Formation of NEDD8~Cul5-Rbx2 covalent conjugate – To obtain the conjugate, E1-activating enzyme APP-BP1/UBA3 (1 µM), E2 conjugating enzyme UBE2F (5 µM), NEDD8 (40 µM), Cul5-Rbx2 (5 µM) were incubated at 37 °C for 1 hour in 50 mM HEPES pH 7.4, 150 mM NaCl, 5 mM DTT, 10 mM $MgCl_2$, 0.2 mM ATP. A negative control experiment was performed in the same solution containing 0.1 mM EDTA, with no $MgCl_2$ or ATP added. The completion of the neddylation on the Cul5 subunit was confirmed by SDS-PAGE (Figure S4).

Size Exclusion Chromatography with inline Multi-Angle Static Light Scattering (SEC-MALS) – SEC-MALS experiments were performed using Dionex Ultimate 3000 UHPLC system (Thermo Scientific) with an inline Wyatt miniDAWN TREOS MALS detector and Optilab T-rEXTM refractive index detector. Molar masses spanning elution peaks were calculated using ASTRA v6.0.0.108 (Wyatt). SEC-MALS data was collected for the following samples: 1) SOCS2-EloBC at 130 µM; 2) Cul5$_{NTD}$ at 110 µM; 3) SOCS2-EloBC-Cul5$_{NTD}$ at 90 µM; 4) Cul5-Rbx2 at 30 µM; 5) SOCS2-EloBC-Cul5-Rbx2 at 35 µM. The experiments were performed using Superdex 200 10/300 GL column (GE Healthcare) with running buffer 50 mM HEPES pH 7.5; 150 mM NaCl; 0.5 mM TCEP. Scattering signal was collected at 44°, 90°, 136° using λ = 658.5 nm incident light. Resulting data were processed in Microsoft Excel and peaks normalized.

Travelling wave ion mobility-mass spectrometry (TWIM-MS) – The native TWIM-MS experiments were conducted on a Synapt HDMS G2 instrument (Waters, Milford, MA, USA) which has been previously described in the literature (21). Samples following gel filtration were buffer exchanged into 500 mM aqueous ammonium acetate at pH 7.0, using Micro Bio-Spin P-6 columns (Bio-Rad), at concentrations in the range of 5-10 µM. Aliquots of 3-5 µL were transferred to gold-coated nanoESI needles prepared in-house. The instrument was tuned to ensure the preservation of non-covalent interactions (22), using the following parameters: capillary 1.2 kV; sample cone 40 V; extraction cone 0.5 V; nanoflow gas pressure 0.3 bar; trap collision energy 4.0 V; transfer collision energy 3.5 V; backing pressure 4 mbar, trap pressure 3.4 mbar. For the measurement of the full 148 kDa complex, SOCS2-EloBC-Cul5-Rbx2, the backing pressure was increased to 5 mbar to facilitate the transmission of high m/z signal. Gas pressure in the ion-mobility cell was 3.0 mbar, He and N_2 gas flows 180 ml/min and 90 ml/min respectively with a trap bias of 50 V. The travelling wave velocity was 800 m/s with a travelling wave height of 40 V. The data were acquired and processed with MassLynx v4.1 software (Waters), and drift times extracted using Driftscope v2.3 (Waters). The experimental collision cross sections (CCS) of the protein complexes were determined by calibration with known protein cross-sections determined under native conditions as described previously (23).

Calculation of Theoretical Collision Cross Sections (CCS) – Theoretical CCS values of the protein complexes were calculated from model structures, obtained by docking individual protein subunits together, using the program MOBCAL with both the projection approximation (PA) and

the exact hard-sphere scattering (EHSS) methods (24, 25). The PDB files were cleaned, i.e. by resolving dihedral conflicts, and adding missing side chains and removing crystal water molecules, prior to the PA or EHSS calculation. The theoretical CCS was compared with the experimental CCS of the lowest available charge state for that species in the mass spectra, which corresponds to the most native-like structure of the protein complex (Figures 4A, 4B and 4C, bottom panels).

Isothermal Titration Calorimetry (ITC) – Experiments were conducted using an iTC200 microcalorimeter instrument (GE Healthcare). GHR_pY595 peptide (350 µM, PVPDpYTSIHIV-amide), GHR_Y595 (350 µM, PVPDYTSIHIV-amide) and phospho-tyrosine (2 mM, pY) were titrated into SOCS2-EloBC (30 µM) at 298 K. Temperature-dependent experiments to study interaction between SOCS2-EloBC and $Cul5_{NTD}$ were performed by titrating $Cul5_{NTD}$ (450 µM) into SOCS2-EloBC (60 µM) at 298, 303 and 308 K. Prior to all titration experiment sample proteins were dialysed into 50 mM HEPES pH 7.5, 250 mM NaCl, 0.5 mM TCEP. Peptides and pY were dissolved in the same buffer. Obtained data were analyzed and fitted using Microcal Origin 7.0 software package. Binding enthalpy, dissociation constants and stoichiometry were determined by fitting the data using a one-set-of-site binding model.

Molecular modeling of protein complexes – Due to the absence of an Rbx2 crystal structure, its closest homolog Rbx1 was used for the model construction. The structural model of the SOCS2-EloBC-Cul5-Rbx1 complex was prepared in PyMol using the crystal structure of Cul1-Rbx1-Skp1-Skp2 (PDB 1LDK) (26) as the initial template. To construct the model, SOCS2-EloBC-$Cul5_{NTD}$ (PDB 4JGH) (12) was superimposed on the template by aligning its $Cul5_{NTD}$ subunit with the $Cul1_{NTD}$ of the template. After that $Cul5_{CTD}$-Rbx1 (PDB 3DPL) (27) was aligned with $Cul1_{CTD}$ subunit of the template to generate a model of the full-length E3 ligase. The resulting model of $CRL5^{SOCS2}$ complex was used to obtain the model for Cul5-Rbx1. To generate a model of the "open" neddylated complexes, NEDD8~$Cul5_{CTD}$-Rbx1 (PDB 3DQV) (27) was aligned with the $Cul1_{CTD}$ subunit of the template. Alternatively, to prepare a model of the "closed" neddylated complexes, NEDD8 was simply added from aligned 3DQV onto the non-neddylated $Cul5_{CTD}$-Rbx1 and SOCS2-EloBC-Cul5-Rbx1.

RESULTS

Components of $CRL5^{SOCS2}$ E3 ligase can be pulled down from human cell lysates using phosphopeptide-modified beads – Specific subunits of E3 ligase SOCS2, EloB, EloC, Cul5 and Rbx2 are known to function as a $CRL5^{SOCS2}$ complex (28). The SH2 domain of SOCS2 recognizes and specifically binds a GHR sequence containing the phosphorylated tyrosine pY595. We envisaged that SOCS2 and components of full-length $CRL5^{SOCS2}$ E3 ligase should be amenable for capturing from cell lysate using substrate peptides immobilized on beads. To this aim we performed pull-down experiments from human K562 cell lysate using beads decorated with both phosphorylated GHR_pY595 (PVPDpYTSIHIV-amide, positive control) and non-phosphorylated GHR_Y595 (PVPDYTSIHIV-amide, negative control) peptides. Mass-spectrometry analysis revealed a reproducible and limited set of proteins captured and subsequently displaced by the phosphorylated peptide (Figure 1A, bottom left corner). All components of the $CRL5^{SOCS2}$ (SOCS2, EloB, EloC, Cul5 and Rbx2) were amongst this protein set.

Binding profile (Figure 1B) shows that endogenous components of $CRL5^{SOCS2}$ E3 ligase were only captured by GHR_pY595-beads. In contrast, no significant capturing from cell lysates was observed with non-phosphorylated GHR_Y595-containing beads (Figure 1B). This observation shows that pY residue plays a key role in recognition of the substrate by the CRL^{SOCS2} complex in the cell and that phosphorylation of the peptide is essential for specific interaction with the E3 ligase. Interestingly, we also detected NEDD8 as a protein specifically pulled by the pY peptide. NEDD8 is a ubiquitin-like protein that is known to be covalently attached to Cullins and acts as a CRL activator by inducing scaffold dynamics and increasing conformational flexibility of the E3 enzyme (27, 29). Identification of NEDD8 suggests that the active neddylated complex is also being pulled down in the assay.

Surprisingly, in addition to the expected $CRL5^{SOCS2}$ complex subunits, we detected

subunits of the $CRL1^{FBXO31}$ E3 ligase, namely FBXO31, Rbx1, Cul1 and Skp1 proteins as being captured by the beads and displaced by the phosphorylated peptide (Figure 1A, Table S1) indicating specific binding. FBXO31 is an F-box protein that binds phosphorylated substrates, therefore it could have been recruited by the GHR_pY595 peptide directly. However, significant recruitment of the four $CRL1^{FBXO31}$ subunits was also observed by the non-phosphorylated GHR peptide (Figure S1). This would imply a degree of phosphorylation-independent interaction, either directly with the beads or indirectly via binding to the components of $CRL5^{SOCS2}$ E3 ligase complex.

Moreover, CSK and CISH proteins were also recruited (Figure 1A, Table S1). Both CSK and CISH contain SH2 domain, therefore both proteins were likely directly recruited by the phosphorylated peptide.

SOCS2-EloBC forms a weak interaction with GHR and a tight interaction with Cul5$_{NTD}$ – To determine the affinity of interaction and the thermodynamic parameters of binding between SOCS2-EloBC and substrate GHR or scaffold $Cul5_{NTD}$ we performed isothermal titration calorimetry experiments (Figure 2). SOCS2-EloBC binds GHR_pY595 peptide with Kd = 1.8 μM, which is consistent with the previously reported value (11), and pY with Kd = 191 μM, both at 298 K (Figure 2A). The binding affinity for phospho-tyrosine is approximately 100-fold weaker than for the phosphorylated peptide suggesting other peptide residues make some contribution to interaction with the protein. However, negative control titration using non-phosphorylated GHR_Y595 peptide showed no binding (Fig. 2A), reinforcing the key contribution of the phosphate group to substrate binding.

We next determined the affinity of SOCS2-EloBC for $Cul5_{NTD}$ by measuring a Kd = 11 nM for the interaction. This data is in good agreement with previously reported Kd = 28 nM (by ITC) (12). In addition, two groups independently reported Kd = 7 nM (by ITC) (30), Kd = 10 nM (by ITC) and Kd = 47 nM (by SPR) (31) for this interaction, albeit using SOCS-box domain instead of the whole SOCS2 protein in complex with EloBC.

To test the potential cooperativity of interactions at the GHR/SOCS2-EloBC/$Cul5_{NTD}$ interfaces we performed titration of GHR_pY595 peptide into SOCS2-EloBC-$Cul5_{NTD}$ and titration of $Cul5_{NTD}$ into GHR_pY595-SOCS2-EloBC complex. No change in the Kd or ΔH values were observed in either cases, suggesting no cooperativity or cross-talk between these interactions.

The interaction between SOCS2-EloBC and Cul5 scaffold is high-affinity and crucial to the assembly of CRL complex. To provide further insights into the nature of this interaction we performed temperature-dependent ITC titrations and determined a change in heat capacity ΔC_P = -450 cal/mol/K (titration curves shown in Figure 2B). Figure 2D demonstrates a plot with temperature-dependent change of thermodynamic parameters of SOCS2-EloBC/$Cul5_{NTD}$ interaction. The experimental ΔC_P value is calculated from the slope of the ΔH linear regression. As a comparison, previously reported ΔC_p values for ASB9-EloBC/$Cul5_{NTD}$ and Vif-EloBC/$Cul5_{NTD}$ interactions were found to be -350 cal/mol/K (18) and -300 cal/mol/K (30), respectively.

We next calculated the theoretical solvent accessible surface area (SASA) values in GetArea (32) and NACCESS (33) software using the crystal structure of SOCS2-EloBC-$Cul5_{NTD}$ complex (PDB 4JGH) as a model (12) (Table 1A). Theoretical ΔC_P values were calculated using the following equation:

$$\Delta C_p = \Delta c_{ap}\Delta ASA_{ap} + \Delta c_p\Delta ASA_p \quad (34),$$

where ΔASA is the apolar (ap) and polar (p) surface buried upon interaction of the proteins and Δc is the area coefficient, representing per $Å^2$ contribution of residues in heat capacity change. The polar and non-polar area coefficients represent values empirically determined from a range of protein data sets by different groups (35-39), reviewed in (34). We observe good agreement between theoretical and experimental data when using area coefficients according to references (39) and (37) (Table 1B).

SOCS2-EloBC forms stable monomeric complexes with Cul5$_{NTD}$ and Cul5-Rbx2 - To validate formation of $CRL5^{SOCS2}$ and determine the stoichiometry of subunits in the complex we demonstrated assembly of the full-length E3 ligase *in vitro* using recombinantly expressed and purified protein components (schematic

representation, Figure 3A). SOCS2 and EloBC were co-expressed in *E. coli* to obtain the SOCS2-EloBC ternary complex and $Cul5_{NTD}$ was independently expressed in *E. coli*. Cul5-Rbx2 protein complex was co-expressed in Sf21 insect cells.

SOCS2-EloBC-$Cul5_{NTD}$ and SOCS2-EloBC-Cul5-Rbx2 protein complexes were formed by mixing SOCS2-EloBC and either $Cul5_{NTD}$ or Cul5-Rbx2 components in equimolar amounts and then purified using size-exclusion chromatography (Figure S2). To validate and characterize the purified protein complexes biophysical analyses were carried out using SEC-MALS, Native MS and TWIM-MS techniques.

The SEC-MALS elution profiles of the different protein components and complexes show that they all exist as monomeric and monodisperse entities (Figure 3D). The molar mass over elution peaks is shown in corresponding colours. Molecular weight values of eluted proteins are summarized in the inset table, Figure 3C. The results of SEC-MALS analysis confirm the formation of expected protein complexes with experimentally determined molecular weights that correlate well with theoretical values.

Experimental collision cross sections for protein complexes are in good agreement with theoretical values – To validate the structural model of SOCS2-EloBC-Cul5-Rbx2, TWIM-MS was used to examine the molecular weight and stoichiometry of the intact protein complexes, as well as confirm their topology by CCS measurements. The protein components SOCS2-EloBC and $Cul5_{NTD}$ alone were first analysed using native MS and the resulting spectra are shown in the Figures S3A and S3B. The masses were confirmed as *ca.* 43 kDa and 45 kDa, respectively. Theoretical and experimental masses for each complex are shown in Table 2.

Combining SOCS2-EloBC with $Cul5_{NTD}$ produced an 89 kDa complex which could be detected with charge states ranging from 16+ to 20+ (Figure 4A). Some free SOCS2-EloBC was also observed in this spectrum, with the same charge states as the native mass spectrum of SOCS2-EloBC alone, indicating that some dissociation in solution occurs (Figure S3). Table 2 shows the experimental CCS values compared to the theoretical ones calculated with the PA and the EHSS methods. It is normally expected that the experimental values would be smaller than the EHSS results and larger than the PA results (24, 25). The collision cross section determined using ion mobility for SOCS2-EloBC-$Cul5_{NTD}$ is 5,092 $Å^2$ for the most native charge state (16+, Figure 5A), which is reasonably close to the theoretical value calculated for the model (Table 2, PA value 5,306 $Å^2$).

A typical spectrum of the Cul5-Rbx2 complex is shown in Figure S3C with a predominant 6+ charge state for Rbx2 and a series of charge states from 19+ to 22+ representing the binary complex (104 kDa). Figure 4B shows the Cul5-Rbx2 complex in more detail in addition to the drift time plot. Moreover, there are less intense peaks to the left hand side of the predominant peak corresponding to a loss of *ca.* 1 kDa from the complex that may represent a truncation in the Cul5 subunit. These species are clearly separated, however, by their ion mobility (Figure 4B), and so it is possible to calculate a collisional cross section for the intact complex. The CCS value from this data for the most native 19+ charge state was found to be 6,061 $Å^2$ (Figure 4B, bottom panel), which compared well to the theoretical value (Table 2, PA value 5,988 $Å^2$).

The native mass spectrum of the SOCS2-EloBC-Cul5-Rbx2 showed intense peaks at 3,000-4,000 m/z, indicating a relative abundance of free SOCS2-EloBC, with charge states 11+ to 13+ as described previously (Figure S3A). It is possible that there is an excess of SOCS2-EloBC in these samples or that this subunit has a greater ionisation efficiency compared to the other protein components. The Figure 4C (bottom panel) depicts the 4,000-7,000 m/z range of the SOCS2-EloBC-Cul5-Rbx2 spectrum that shows peaks ranging from 4,300-4,900 m/z representing a small amount of SOCS2-EloBC dimer. Secondly, at 4,700-5,600 m/z the Cul5-Rbx2 complex is detected with charge states from 19+ to 22+. Finally, the peaks representing the full 148 kDa complex, SOCS2-EloBC-Cul5-Rbx2, are in the range of 5,600-6,600 m/z, with charge states 23+ to 26+.

The CCS values measured for each charge state of the full 148 kDa complex are displayed in Figure 4C, bottom panel. For the lowest charge state of SOCS2-EloBC-Cul5-Rbx2, an experimental cross section of 7,653 $Å^2$ was determined compared to a theoretical CCS of 7,918 $Å^2$ (Table 2), confirming the structural

model as shown in Figure S6D. In this case the experimentally determined value is slightly smaller than the theoretical value, which could indicate that the structure is slightly more compact than the model suggests.

To investigate the effect of neddylation on the complex assembly, we performed *in vitro* neddylation assays on the purified Cul5-Rbx2 complex and used the reaction product NEDD8~Cul5-Rbx2 to reconstitute neddylated full complex SOCS2-EloBC-Cul5-Rbx2. The masses for these neddylated complexes (Table 2, 113 kDa and 157 kDa respectively) are in agreement with the theoretical mass for addition of NEDD8. Firstly, the same range of charge states was observed for the non-neddylated and neddylated complexes in the native mass spectra (Figure S5). This would indicate that no significant conformational rearrangement had occurred. Secondly, the CCS values measured by TWIM-MS for each charge state of the neddylated complexes were compared with those of the non-neddylated ones (Figure 5A and 5B), showing an increase in CCS of 150-200 $Å^2$ in each case. We compared the experimental data with two alternative models; one "open" model which assumes a conformational change upon neddylation, and another "closed" model which simply has NEDD8 added onto the non-neddylated complex, with the aim to distinguish them based on the TWIM-MS data. The calculated CCS increase for the two alternative neddylated models (NEDD8~Cul5-Rbx1) vs. the non-neddylated one (Figure S6), is 350 $Å^2$ for the "closed" model and 523 $Å^2$ for the "open" model (PA method, Table 2). Whereas, for SOCS2-EloBC-NEDD8~Cul5-Rbx1 the neddylation accounts for an extra 312 $Å^2$ ("closed") and 415 $Å^2$ ("open"). It would therefore appear that the increase in size is predominantly due to the addition of NEDD8 rather than a significant conformational change.

DISCUSSION

Here, we show that all $CRL5^{SOCS2}$ components SOCS2, EloBC, Cul5 and Rbx2 can be specifically pulled down from the human cell lysates with subsequent validation of their identity by MS analysis. These components were recombinantly expressed and purified, and then assembled *in vitro* into different sized complexes up to the full-size E3 ligase.

Biophysical studies of the full-size CRLs are important for better understanding the principles of assembly and gaining insight into their structural architecture. This is particularly relevant for the cases where crystal structures are not available, as it is for $CRL5^{SOCS2}$. We addressed this by presenting the first report of *in vitro* assembly of full-size human $CRL5^{SOCS2}$ reconstituted from recombinant components, and provide a biophysical analysis of the obtained complexes.

The structural model of SOCS2-EloBC-Cul5-Rbx2 complex was validated by TWIM-MS studies. The experimentally measured CCS values are in agreement with the theoretically calculated ones, although the molecular architecture of SOCS2-EloBC-$Cul5_{NTD}$ and SOCS2-EloBC-Cul5-Rbx2 appears to be slightly more compact than predicted.

Modification of the Cullin scaffold with NEDD8 protein is crucial for the activation of CRLs (40). Previous structural studies showed that NEDD8 promotes a conformational rearrangement of the Cul1-Rbx1 component of CRL1 (27). Such a structural alteration enables Rbx1-E2~Ub to extend towards the substrate receptor subunit, thereby promoting substrate polyubiquitination. One of the proteins identified in the pull-down experiments was NEDD8, supporting the presence of the active neddylated complex inside cells. Comparison of TWIM-MS data between neddylated and non-neddylated Cul5-Rbx2 and SOCS2-EloBC-Cul5-Rbx2 complexes showed an increase of 150-200 $Å^2$ in CCS values (Table 2). Interestingly, the increase in calculated CCS values defined by the addition of NEDD8 is ~ 2–3 times larger than the conformational change of the Rbx1 subunit in the "open" models (Figures S6C and S6F). Therefore, the difference between "open" and "closed" neddylated models is not significant enough, and therefore we cannot distinguish them based on the experimental data. The observed change in CCS is largely due to the addition of the extra NEDD8 subunit.

One of the main limitations towards biophysical studies of the whole multi-subunit CRLs is the difficulty of obtaining all the components in appropriate amount and quality, particularly full-length Cullins. Expression and

purification of stable full-length Cullin scaffolds in complex with RING domain proteins is not trivial and has been previously reported only for Cul1-Rbx1 (26), Cul4A-Rbx1 (41), Cul4B-Rbx1 (42) and Cul5-Rbx2 (20). As a result, there were only a few cases in the literature describing characterization of the full-size CRLs assembled from recombinant subunits (26, 42). To purify the Cul5-Rbx2 complex in this study we used the Dac-tag technology that provides additional stability and solubility to the protein complex and additionally improves the yield of recombinant proteins (19). This approach has also proven to be successful for purification of Cul2-Rbx1 complex (A.K., personal communication) and could be further extended to other Cullins and large multi-subunit complexes.

In certain cases CRLs exist and function in homo- or hetero-oligomeric states. For example, several studies have shown that CRL3 can dimerize via an adaptor BTB domain (43) or through NEDD8-mediated interaction between two Cul3 scaffolds (44). CRL1 was also demonstrated to be able to dimerize via the receptor Cdc4 resulting in enhanced ubiquitination of substrate Sic1 (45). In our case, however, using SEC-MALS and native MS techniques we established that the $CRL5^{SOCS2}$ exists in a monomeric state.

Our measured Kd values for the interaction of SOCS2-EloBC with GHR_pY595 peptide or $Cul5_{NTD}$ are in good agreement with previously reported data (11, 31). Weak SOCS2-EloBC/GHR_pY595 interaction (Kd = 1.8 μM) could suggest low selectivity towards a particular substrate and instead ability to target a variety of phosphorylated proteins. In contrast, the interaction of SOCS2-EloBC with scaffold $Cul5_{NTD}$ is very tight (Kd = 11 nM, at 298 K). The large negative ΔC_P value (-450 cal/mol/K) for the SOCS2-EloBC/$Cul5_{NTD}$ interaction indicates a major contribution of the hydrophobic interface and further reflects the high affinity (34, 38), e.g. when compared with other related interactions such as ASB9-EloBC/$Cul5_{NTD}$ and Vif-EloBC/$Cul5_{NTD}$ (18, 30). Overall, these results indicate the structural importance of the SOCS2-EloBC/$Cul5_{NTD}$ interface for assembly and stability of the $CRL5^{SOCS2}$.

As the next logical step following the current study, we believe it would be important to develop an assay to measure activity of the recombinant $CRL5^{SOCS2}$ against the substrate GHR protein resulting in ubiquitination and the subsequent proteasomal degradation of the latter. Such an assay could be useful for testing the potency of small molecule modulators of $CRL5^{SOCS2}$ activity. In accordance with this, a recent example demonstrates *in vitro* reconstitution of murine $CRL5^{SOCS3}$, containing SOCS3, a close homolog of SOCS2, as a substrate receptor subunit (46). The authors used co-expressed $Cul5_{NTD}$, $Cul5_{CTD}$ and Rbx2 proteins to form a complex with SOCS3-EloBC, and the assembled E3 ligase then demonstrated activity in ubiquitination assay against substrates JAK2 and gp130.

In addition, it would be important to obtain the crystal structure of the receptor SOCS2 bound to the substrate GHR depicting the details of the interface between two proteins. This could substantially advance the development of inhibitors of this interaction, i.e. structural phospho-tyrosine analogs or isosteres. The biophysical insights to the interactions and assembly of the full-size $CRL5^{SOCS2}$ E3 ligase reported in our study will aid future developments in this direction.

REFERENCES

1. Sarikas, A., Hartmann, T., and Pan, Z.-Q. (2011) The cullin protein family. *Genome Biol.* **12**, 220
2. Soucy, T. A., Smith, P. G., Milhollen, M. A., Berger, A. J., Gavin, J. M., Adhikari, S., Brownell, J. E., Burke, K. E., Cardin, D. P., Critchley, S., Cullis, C. A., Doucette, A., Garnsey, J. J., Gaulin, J. L., Gershman, R. E., Lublinsky, A. R., McDonald, A., Mizutani, H., Narayanan, U., Olhava, E. J., Peluso, S., Rezaei, M., Sintchak, M. D., Talreja, T., Thomas, M. P., Traore, T., Vyskocil, S., Weatherhead, G. S., Yu, J., Zhang, J., Dick, L. R., Claiborne, C. F., Rolfe, M., Bolen, J. B., and Langston, S. P. (2009) An inhibitor of NEDD8-activating enzyme as a new approach to treat cancer. *Nature* **458**, 732–736
3. Feldman, R. M., Correll, C. C., Kaplan, K. B., and Deshaies, R. J. (1997) A complex of Cdc4p, Skp1p, and Cdc53p/cullin catalyzes ubiquitination of the phosphorylated CDK inhibitor Sic1p. *Cell* **91**, 221–230
4. Bosu, D. R., and Kipreos, E. T. (2008) Cullin-RING ubiquitin ligases: global regulation and activation cycles. *Cell Div* **3**, 7
5. Lydeard, J. R., Schulman, B. A., and Harper, J. W. (2013) Building and remodelling Cullin-RING E3 ubiquitin ligases. *EMBO Rep.* **14**, 1050–1061
6. Zimmerman, E. S., Schulman, B. A., and Zheng, N. (2010) Structural assembly of cullin-RING ubiquitin ligase complexes. *Curr. Opin. Struct. Biol.* **20**, 714–721
7. Kamura, T., Maenaka, K., Kotoshiba, S., Matsumoto, M., Kohda, D., Conaway, R. C., Conaway, J. W., and Nakayama, K. I. (2004) VHL-box and SOCS-box domains determine binding specificity for Cul2-Rbx1 and Cul5-Rbx2 modules of ubiquitin ligases. *Genes Dev.* **18**, 3055–3065
8. Mahrour, N., Redwine, W. B., Florens, L., Swanson, S. K., Martin-Brown, S., Bradford, W. D., Staehling-Hampton, K., Washburn, M. P., Conaway, R. C., and Conaway, J. W. (2008) Characterization of Cullin-box sequences that direct recruitment of Cul2-Rbx1 and Cul5-Rbx2 modules to Elongin BC-based ubiquitin ligases. *J. Biol. Chem.* **283**, 8005–8013
9. Greenhalgh, C. J., Rico-Bautista, E., Lorentzon, M., Thaus, A. L., Morgan, P. O., Willson, T. A., Zervoudakis, P., Metcalf, D., Street, I., Nicola, N. A., Nash, A. D., Fabri, L. J., Norstedt, G., Ohlsson, C., Flores-Morales, A., Alexander, W. S., and Hilton, D. J. (2005) SOCS2 negatively regulates growth hormone action in vitro and in vivo. *J. Clin. Invest.* **115**, 397–406
10. Greenhalgh, C. J., Metcalf, D., Thaus, A. L., Corbin, J. E., Uren, R., Morgan, P. O., Fabri, L. J., Zhang, J.-G., Martin, H. M., Willson, T. A., Billestrup, N., Nicola, N. A., Baca, M., Alexander, W. S., and Hilton, D. J. (2002) Biological evidence that SOCS-2 can act either as an enhancer or suppressor of growth hormone signaling. *J. Biol. Chem.* **277**, 40181–40184
11. Bullock, A. N., Debreczeni, J. É., Edwards, A. M., Sundström, M., and Knapp, S. (2006) Crystal structure of the SOCS2-elongin C-elongin B complex defines a prototypical SOCS box ubiquitin ligase. *Proc. Natl. Acad. Sci. U.S.A.* **103**, 7637–7642
12. Kim, Y. K., Kwak, M.-J., Ku, B., Suh, H.-Y., Joo, K., Lee, J., Jung, J. U., and Oh, B.-H. (2013) Structural basis of intersubunit recognition in elongin BC–cullin 5–SOCS box ubiquitin–protein ligase complexes. *Acta Crystallogr Sect D Biol Crystallogr* **69**, 1587–1597
13. Cohen, P., and Tcherpakov, M. (2010) Will the ubiquitin system furnish as many drug targets as protein kinases? *Cell* **143**, 686–693
14. Petroski, M. D. (2008) The ubiquitin system, disease, and drug discovery. *BMC Biochem.* **9 Suppl 1**, S7
15. Andérica-Romero, A. C., González-Herrera, I. G., Santamaría, A., and Pedraza-Chaverri, J. (2013) Cullin 3 as a novel target in diverse pathologies. *Redox Biol* **1**, 366–372
16. Zhao, Y., and Sun, Y. (2013) Cullin-RING Ligases as attractive anti-cancer targets. *Curr. Pharm. Des.* **19**, 3215–3225
17. Bantscheff, M., Hopf, C., Savitski, M. M., Dittmann, A., Grandi, P., Michon, A.-M., Schlegl, J., Abraham, Y., Becher, I., Bergamini, G., Boesche, M., Delling, M., Dümpelfeld, B., Eberhard, D., Huthmacher, C., Mathieson, T., Poeckel, D., Reader, V., Strunk, K., Sweetman, G., Kruse, U.,

Neubauer, G., Ramsden, N. G., and Drewes, G. (2011) Chemoproteomics profiling of HDAC inhibitors reveals selective targeting of HDAC complexes. *Nat. Biotechnol.* **29**, 255–265
18. Thomas, J. C., Matak-Vinkovic, D., Van Molle, I., and Ciulli, A. (2013) Multimeric complexes among ankyrin-repeat and SOCS-box protein 9 (ASB9), ElonginBC, and Cullin 5: insights into the structure and assembly of ECS-type Cullin-RING E3 ubiquitin ligases. *Biochemistry* **52**, 5236–5246
19. Lee, D. W., Peggie, M., Deak, M., Toth, R., Gage, Z. O., Wood, N., Schilde, C., Kurz, T., and Knebel, A. (2012) The Dac-tag, an affinity tag based on penicillin-binding protein 5. *Anal. Biochem.* **428**, 64–72
20. Kelsall, I. R., Duda, D. M., Olszewski, J. L., Hofmann, K., Knebel, A., Langevin, F., Wood, N., Wightman, M., Schulman, B. A., and Alpi, A. F. (2013) TRIAD1 and HHARI bind to and are activated by distinct neddylated Cullin-RING ligase complexes. *EMBO J.* **32**, 2848–2860
21. Pringle, S. D., Giles, K., Wildgoose, J. L., Williams, J. P., Slade, S. E., Thalassinos, K., Bateman, R. H., Bowers, M. T., and Scrivens, J. H. (2007) An investigation of the mobility separation of some peptide and protein ions using a new hybrid quadrupole/travelling wave IMS/oa-ToF instrument. *International Journal of Mass Spectrometry* **261**, 1–12
22. Konijnenberg, A., Butterer, A., and Sobott, F. (2013) Native ion mobility-mass spectrometry and related methods in structural biology. *Biochim. Biophys. Acta* **1834**, 1239–1256
23. Bush, M. F., Hall, Z., Giles, K., Hoyes, J., Robinson, C. V., and Ruotolo, B. T. (2010) Collision cross sections of proteins and their complexes: a calibration framework and database for gas-phase structural biology. *Anal. Chem.* **82**, 9557–9565
24. Mesleh, M. F., Hunter, J. M., Shvartsburg, A. A., Schatz, G. C., and Jarrold, M. F. (1996) Structural Information from Ion Mobility Measurements: Effects of the Long-Range Potential. *J. Phys. Chem.* **100**, 16082–16086
25. Shvartsburg, A. A., and Jarrold, M. F. (1996) An exact hard-spheres scattering model for the mobilities of polyatomic ions. *Chemical Physics Letters* **261**, 86–91
26. Zheng, N., Schulman, B. A., Song, L., Miller, J. J., Jeffrey, P. D., Wang, P., Chu, C., Koepp, D. M., Elledge, S. J., Pagano, M., Conaway, R. C., Conaway, J. W., Harper, J. W., and Pavletich, N. P. (2002) Structure of the Cul1-Rbx1-Skp1-F boxSkp2 SCF ubiquitin ligase complex. *Nature* **416**, 703–709
27. Duda, D. M., Borg, L. A., Scott, D. C., Hunt, H. W., Hammel, M., and Schulman, B. A. (2008) Structural insights into NEDD8 activation of cullin-RING ligases: conformational control of conjugation. *Cell* **134**, 995–1006
28. Vesterlund, M., Zadjali, F., Persson, T., Nielsen, M. L., Kessler, B. M., Norstedt, G., and Flores-Morales, A. (2011) The SOCS2 ubiquitin ligase complex regulates growth hormone receptor levels. *PLoS ONE* **6**, e25358
29. Pan, Z.-Q., Kentsis, A., Dias, D. C., Yamoah, K., and Wu, K. (2004) Nedd8 on cullin: building an expressway to protein destruction. *Oncogene* **23**, 1985–1997
30. Salter, J. D., Lippa, G. M., Belashov, I. A., and Wedekind, J. E. (2012) Core-binding factor β increases the affinity between human Cullin 5 and HIV-1 Vif within an E3 ligase complex. *Biochemistry* **51**, 8702–8704
31. Babon, J. J., Sabo, J. K., Zhang, J.-G., Nicola, N. A., and Norton, R. S. (2009) The SOCS box encodes a hierarchy of affinities for Cullin5: implications for ubiquitin ligase formation and cytokine signalling suppression. *J. Mol. Biol.* **387**, 162–174
32. Fraczkiewicz, R., and Braun, W. (1998) Exact and efficient analytical calculation of the accessible surface areas and their gradients for macromolecules. *Journal of Computational Chemistry* **19**, 319
33. Hubbard, S. J., and Thornton, J. M. (1993) NACCESS, Computer Program, Department of Biochemistry and Molecular Biology, University College London.
34. Prabhu, N. V., and Sharp, K. A. (2005) Heat capacity in proteins. *Annu Rev Phys Chem* **56**, 521–548
35. Spolar, R. S., Livingstone, J. R., and Record, M. T. (1992) Use of liquid hydrocarbon and amide

transfer data to estimate contributions to thermodynamic functions of protein folding from the removal of nonpolar and polar surface from water. *Biochemistry* **31**, 3947–3955
36. Myers, J. K., Pace, C. N., and Scholtz, J. M. (1995) Denaturant m values and heat capacity changes: relation to changes in accessible surface areas of protein unfolding. *Protein Sci.* **4**, 2138–2148
37. Makhatadze, G. I., and Privalov, P. L. (1995) Energetics of protein structure. *Adv. Protein Chem.* **47**, 307–425
38. Robertson, A. D., and Murphy, K. P. (1997) Protein Structure and the Energetics of Protein Stability. *Chem. Rev.* **97**, 1251–1268
39. Murphy, K. P., and Freire, E. (1992) Thermodynamics of structural stability and cooperative folding behavior in proteins. *Adv. Protein Chem.* **43**, 313–361
40. Read, M. A., Brownell, J. E., Gladysheva, T. B., Hottelet, M., Parent, L. A., Coggins, M. B., Pierce, J. W., Podust, V. N., Luo, R. S., Chau, V., and Palombella, V. J. (2000) Nedd8 modification of cul-1 activates SCF(beta(TrCP))-dependent ubiquitination of IkappaBalpha. *Mol. Cell. Biol.* **20**, 2326–2333
41. Angers, S., Li, T., Yi, X., MacCoss, M. J., Moon, R. T., and Zheng, N. (2006) Molecular architecture and assembly of the DDB1-CUL4A ubiquitin ligase machinery. *Nature* **443**, 590–593
42. Fischer, E. S., Scrima, A., Böhm, K., Matsumoto, S., Lingaraju, G. M., Faty, M., Yasuda, T., Cavadini, S., Wakasugi, M., Hanaoka, F., Iwai, S., Gut, H., Sugasawa, K., and Thomä, N. H. (2011) The molecular basis of CRL4DDB2/CSA ubiquitin ligase architecture, targeting, and activation. *Cell* **147**, 1024–1039
43. Chew, E.-H., Poobalasingam, T., Hawkey, C. J., and Hagen, T. (2007) Characterization of cullin-based E3 ubiquitin ligases in intact mammalian cells--evidence for cullin dimerization. *Cell. Signal.* **19**, 1071–1080
44. Wimuttisuk, W., and Singer, J. D. (2007) The Cullin3 ubiquitin ligase functions as a Nedd8-bound heterodimer. *Mol. Biol. Cell* **18**, 899–909
45. Tang, X., Orlicky, S., Lin, Z., Willems, A., Neculai, D., Ceccarelli, D., Mercurio, F., Shilton, B. H., Sicheri, F., and Tyers, M. (2007) Suprafacial orientation of the SCFCdc4 dimer accommodates multiple geometries for substrate ubiquitination. *Cell* **129**, 1165–1176
46. Kershaw, N. J., Laktyushin, A., Nicola, N. A., and Babon, J. J. (2014) Reconstruction of an active SOCS3-based E3 ubiquitin ligase complex in vitro: identification of the active components and JAK2 and gp130 as substrates. *Growth Factors* **32**, 1–10

Acknowledgements - We are grateful to the UK Biotechnology and Biological Sciences Research Council (BBSRC BB/G023123/1 David Phillips Fellowship to A.C.); European Research Council (ERC Starting Grant ERC-2012-StG-311460 DrugE3CRLs to A.C.) and Government of the Republic of Tatarstan (PhD studentship to E.B.) for funding. We thank Colin Hammond and Prof. Tom Owen-Hughes (College of Life Sciences, University of Dundee) for assistance with SEC-MALS experiments. F.S. is a Francqui Research Professor at UA. The Synapt G2 mass spectrometer is funded by a grant from the Hercules Foundation – Flanders.

FOOTNOTES

The abbreviations used are: BTB, bric-a-brac/tram-track/broad complex; CCS, collision cross section; Cdc4, cell division control protein 4; CISH, cytokine-inducible SH2-containing protein;CRL, Cullin-RING E3 ubiquitin ligase; $CRL5^{SOCS2}$, SOCS2-EloBC-Cul5-Rbx2 complex; CSK, C-terminal Src kinase; CTD, C-terminal domain; Cul5, Cullin5; DCAF, DDB1 and Cul4-associated factor; DDB1, DNA damage-binding protein 1; EGTA, [Ethylenebis(oxyethylenenitrilo)]tetraacetic acid; EloB, ElonginB; EloC, ElonginC; EloBC, ElonginB-ElonginC complex; EHSS, exact hard-sphere scattering; FBXO31, F-box only protein 31; GHR, growth hormone receptor; HEPES, 4-(2-hydroxyethyl)-1-piperazineethanesulfonic acid; TWIM-MS, travelling wave ion mobility-mass spectrometry; IPTG, isopropyl β-D-1-thiogalactopyranoside; ITC, isothermal titration calorimetry; NEDD8, neural precursor cell expressed developmentally down-regulated protein 8; NTD, N-terminal domain; PA, projection approximation; Rbx, RING-box protein; RING, really interesting new gene; RMSD, root-mean-square deviation; SASA, solvent accessible surface area; Skp, S-phase kinase-associated protein; SDS-PAGE, sodium dodecyl sulfate polyacrylamide gel electrophoresis; SEC-MALS, size exclusion chromatography and multi-angle light scattering; SOCS2, suppressor of cytokine signaling 2; SPR, surface plasmon resonance; TCEP, tris(2-carboxyethyl) phosphine hydrochloride; TEV, tobacco etch virus.

FIGURE LEGENDS

FIGURE 1. Components of $CRL5^{SOCS2}$ E3 ligase can be captured from cell lysate using phosphorylated substrate peptide attached to the beads. *A,* Scattered plot of the peptide pull-down experiments after MS analysis: log2 fold changes of all proteins captured on the phosphorylated GHR_pY595 peptide beads after competition with 100 μM of the same peptide in the lysate. Each protein is indicated by a circle and the size of the circle is proportional to the MS1 value. The labeled proteins are at least 50% displaced by the addition of the peptide in both experiments (log2 fold change ≤1, orange dotted lines). *B,* Relative binding profile of the components of $CRL5^{SOCS2}$ E3 ligase complex captured on the beads decorated with phosphorylated (pY) vs. non-phosphorylated (Y) GHR_(p)Y595 peptide.

FIGURE 2. ITC data demonstrates weak interaction of SOCS2-EloBC with phosphorylated substrate GHR and tight interaction with scaffold $Cul5_{NTD}$. *A,* ITC titration curves of 350 μM GHR peptides (left) and 2 mM pY (right) into 30 μM SOCS2-EloBC protein at 298 K. Phosphorylated GHR_pY595 peptide (black squares), and non-phosphorylated GHR_Y595 (white circles) are shown left. *B,* Titration curves for temperature-dependent ITC of 450 μM $Cul5_{NTD}$ into 60 μM SOCS2-EloBC at 298 (left), 303 (middle) and 308 K (right). *C,* Table summarizing data obtained from ITC experiments. *D,* Plot demonstrating temperature dependence of thermodynamic parameters and calculation of heat capacity (ΔC_P) for SOCS2-EloBC/$Cul5_{NTD}$ interaction.

FIGURE 3. Recombinant components of $CRL5^{SOCS2}$ assemble into the monomeric full-size protein complex. *A,* Schematic representation of $CRL5^{SOCS2}$ that includes substrate receptor SOCS2, adaptor EloBC complex, scaffold Cul5 and RING domain protein Rbx2. *B,* SDS-PAGE gel images of the purified protein complexes. *C,* Table showing comparison of theoretical protein molecular weights against values experimentally determined by SEC-MALS. *D,* SEC-MALS elution profiles for the individual components of $CRL5^{SOCS2}$ and their complexes, including full-size SOCS2-EloBC-Cul5-Rbx2 complex.

FIGURE 4. Ion mobility drift-time plot (top), corresponding native mass spectra (middle) and collision cross sections (bottom) are shown for the $CRL5^{SOCS2}$ complexes and their components. *A,* SOCS2-EloBC-$Cul5_{NTD}$; *B,* Cul5-Rbx2; *C,* the full-size complex SOCS2-EloBC-Cul5-Rbx2.

FIGURE 5. Experimental ion mobility data for a range of charge states suggests an increase in CCS values upon neddylation of the protein complexes. Collision cross sections for *A,* Cul5-Rbx2 and NEDD8~Cul5-Rbx2; *B,* SOCS2-EloBC-Cul5-Rbx2 and SOCS2-EloBC-NEDD8~Cul5-Rbx2. "Closed" conformation model of neddylated complexes *C,* NEDD8~Cul5-Rbx1; *D,* SOCS2-EloBC-NEDD8~Cul5-Rbx1.

TABLE 1. Large negative ΔC_P value for SOCS2-EloBC/$Cul5_{NTD}$ interaction indicates a highly hydrophobic interface between the proteins. *A,* Theoretical ΔSASA values for SOCS2-EloBC/$Cul5_{NTD}$ interaction calculated using GetArea and NACCESS programs. *B,* Comparison between theoretical and experimental ΔC_P values shows good agreement.

TABLE 2. Summary of the experimental and theoretical CCS data. Masses measured for the protein complexes and observed charge state ranges. Comparison of experimental CCS values of the protein complexes vs. their theoretical values calculated using PA and the EHSS methods. Presented data also includes calculated theoretical CCS values for "open" and "closed" NEDD~Cul5-Rbx1 and SOCS2-EloBC-NEDD~Cul5-Rbx1 complexes.

FIGURE 1.

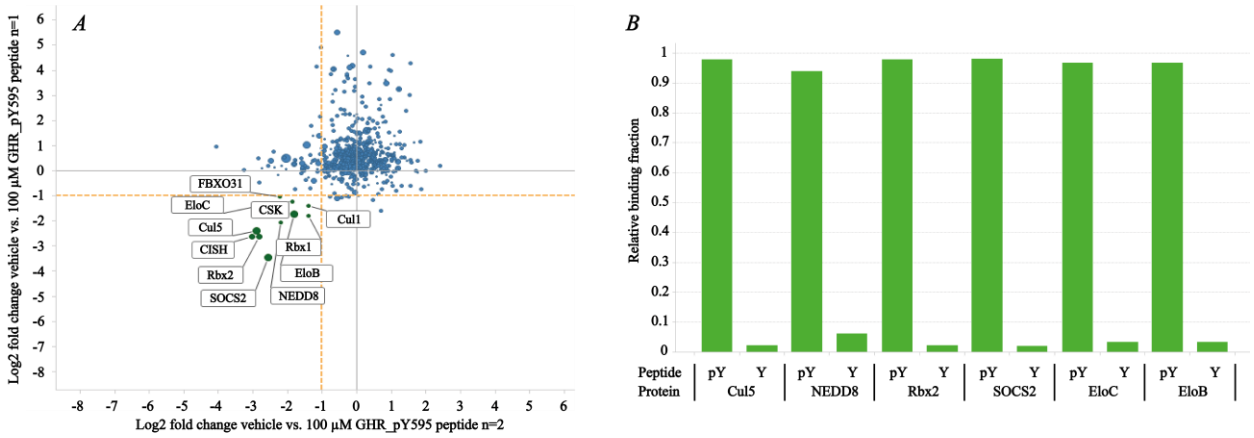
A
Log2 fold change vehicle vs. 100 µM GHR_pY595 peptide n=1
Log2 fold change vehicle vs. 100 µM GHR_pY595 peptide n=2
FBXO31
EloC
CSK
Cul1
Cul5
CISH
Rbx1
Rbx2
EloB
SOCS2
NEDD8
B
Relative binding fraction
Peptide
Protein
pY
Y
Cul5
NEDD8
Rbx2
SOCS2
EloC
EloB

FIGURE 2.

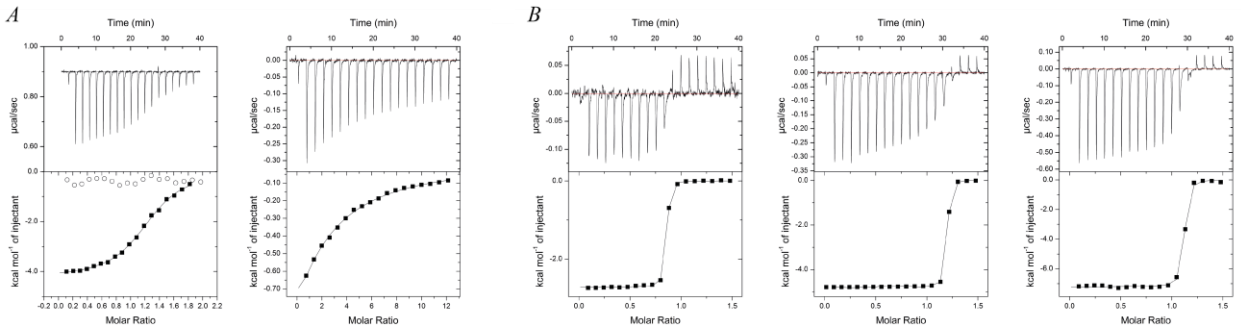

C

Material in Syringe	Material in Cell	T (K)	N	Kd (µM)	ΔH (cal/mol)	-TΔS (cal/mol)	ΔG (cal/mol)
GHR_pY595	SOCS2-EloBC	298	1.2	1.8 ± 0.1	-4,227 ± 32	-3603 ± 66	-7,839 ± 34
pY	SOCS2-EloBC	298	1.0	191 ± 4.0	-4,856 ± 54	-214 ± 66	-5070 ± 12
$Cul5_{NTD}$	SOCS2-EloBC	298	0.8	11.3 ± 1.6	-2,714 ± 6	-8,127 ± 91	-10,841 ± 84
$Cul5_{NTD}$	SOCS2-EloBC	303	1.2	5.6 ± 1.0	-4,788 ± 8	-6,661 ± 116	-11,449 ± 109
$Cul5_{NTD}$	SOCS2-EloBC	308	1.1	19.7 ± 4.3	-7,218 ± 27	-3,655 ± 163	-10,873 ± 136

D

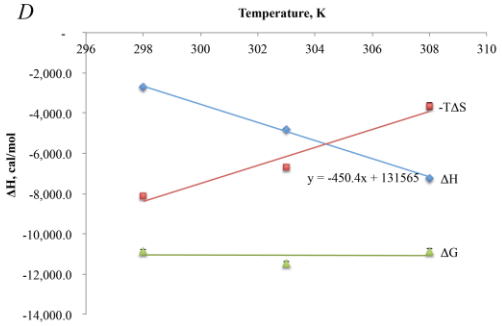

FIGURE 3.

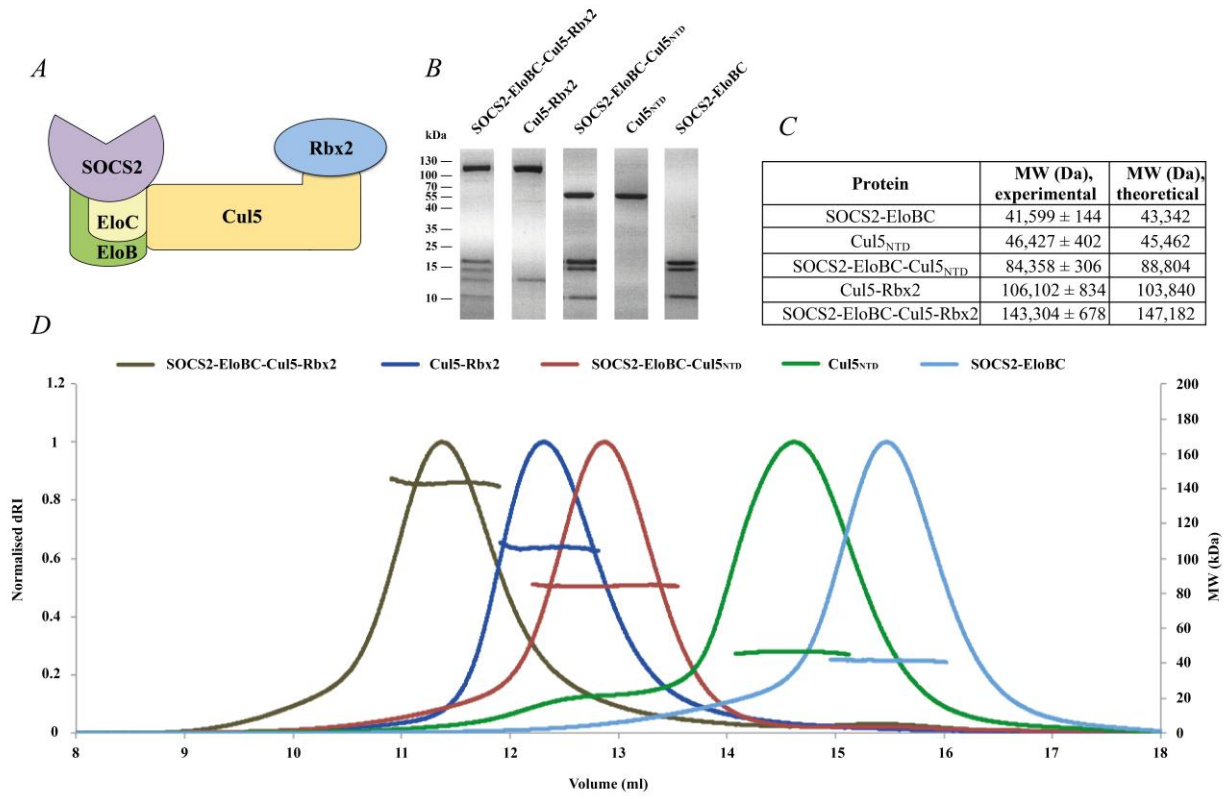
A
SOCS2
Rbx2
EloC
Cul5
EloB
B
kDa
SOCS2-EloBC-Cul5-Rbx2
Cul5-Rbx2
SOCS2-EloBC-Cul5NTD
Cul5NTD
SOCS2-EloBC
130
100
70
55
40
35
25
15
10
C
Protein | MW (Da), experimental | MW (Da), theoretical
SOCS2-EloBC | 41,599 ± 144 | 43,342
Cul5NTD | 46,427 ± 402 | 45,462
SOCS2-EloBC-Cul5NTD | 84,358 ± 306 | 88,804
Cul5-Rbx2 | 106,102 ± 834 | 103,840
SOCS2-EloBC-Cul5-Rbx2 | 143,304 ± 678 | 147,182
D
SOCS2-EloBC-Cul5-Rbx2
Cul5-Rbx2
SOCS2-EloBC-Cul5NTD
Cul5NTD
SOCS2-EloBC
Normalised dRI
MW (kDa)
Volume (ml)

FIGURE 4.

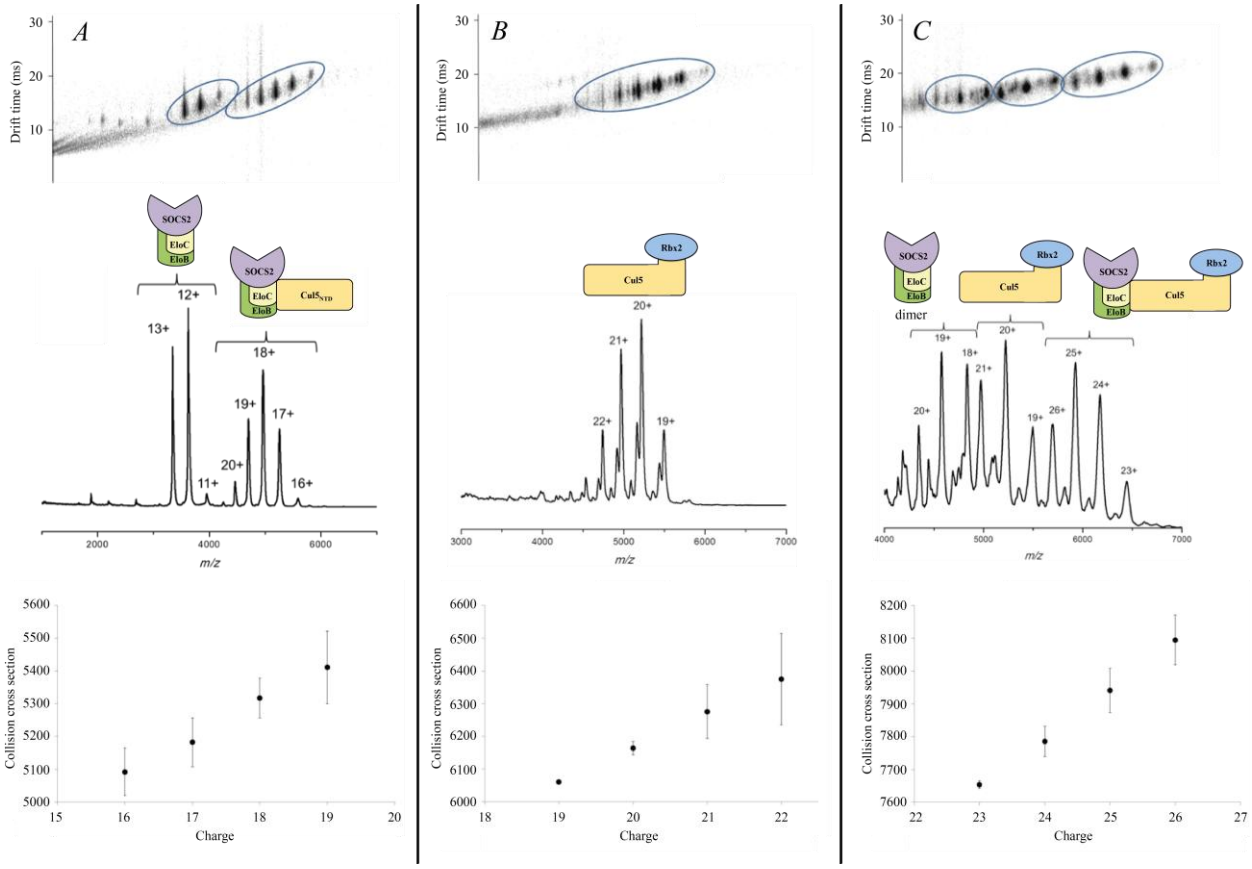
A
B
C
Drift time (ms)
SOCS2
EloC
EloB
Cul5 N-TD
Rbx2
Cul5
dimer
m/z
Collision cross section
Charge

FIGURE 5.

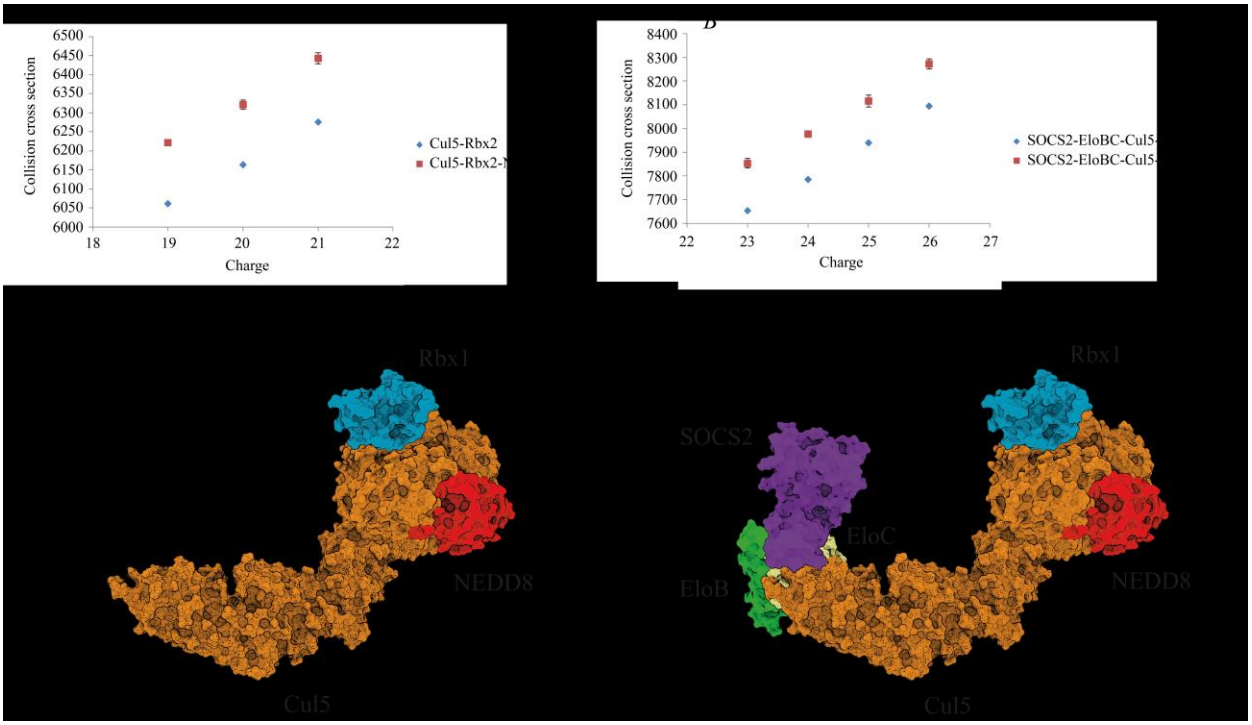
Collision cross section
Charge
Cul5-Rbx2
Cul5-Rbx2-
Rbx1
NEDD8
Cul5
B
Collision cross section
Charge
SOCS2-EloBC-Cul5-
SOCS2-EloBC-Cul5-
Rbx1
SOCS2
EloC
EloB
NEDD8
Cul5

TABLE 1.

A

		SASA (Å^2)			ΔSASA (Å^2)		
		Polar	Apolar	Total	Polar	Apolar	Total
GetArea	SOCS2-EloBC	7,270.0	10,908.7	18,178.7			
	$Cul5_{NTD}$	7,709.6	11,708.7	19,418.4			
	SOCS2-EloBC-$Cul5_{NTD}$	14,361.0	21,291.4	35,652.5	-618.6	-1,326.0	-1,944.6
NACCESS	SOCS2-EloBC	7,992.5	10,375.8	18,368.3			
	$Cul5_{NTD}$	8,393.4	11,216.6	19,610.0			
	SOCS2-EloBC-$Cul5_{NTD}$	15,688.9	20,378.7	36,067.6	-697.0	-1,213.7	-1,910.7

B

		ΔC_p (cal/mol/K)	
	Source	GetArea	NACCESS
experimental		-450.0	
theoretical	Spolar et. al.	-337.5	-290.4
	Murphy and Friere	-434.7	-363.8
	Myers	-314.6	-276.1
	Makharadze and Privalov	-548.1	-474.2
	Robertson and Murphy	-286.0	-278.1

TABLE 2.

Protein	Theoretical mass (Da)	Experimental mass (Da)	Charge states	Theoretical CCS (Å^2)		Experimental CCS (Å^2)
				PA	EHSS	
SOCS2-EloBC	43,341.6	43,566.5	11^+ - 13^+			
$Cul5_{NTD}$	45,462.0	45,612.8	12^+ - 15^+			
SOCS2-EloBC-$Cul5_{NTD}$	88,803.6	89,275.1	16^+ - 20^+	5,306	6,844	5,092
Cul5-Rbx1/2	103,840.0	104,218.8	19^+ - 23^+	5,988	7,822	6,061
SOCS2-EloBC-Cul5-Rbx1/2	147,181.6	148,121.5	23^+ - 26^+	7,918	10,298	7,653
				"Open" / "Closed"	**"Open" / "Closed"**	
NEDD8~Cul5-Rbx1/2	112,911.9	112,981.3	19^+ - 22^+	6,511 / 6,338	8,491 / 8,288	6,222
SOCS2-EloBC-NEDD8~Cul5-Rbx1/2	156,253.5	157,000.0	23^+ - 26^+	8,333 / 8,230	10,843 / 10,701	7,853

SUPPLEMENTARY MATERIALS

FIGURE S1. Fractional binding to phosphorylated GHR_pY595 vs. non-phosphorylated GHR_Y595-modified beads of all proteins that are specifically enriched on GHR_pY595 beads (see Figure 1A). Components of the CRL5^{SOCS2} E3 ligase are coloured in green.

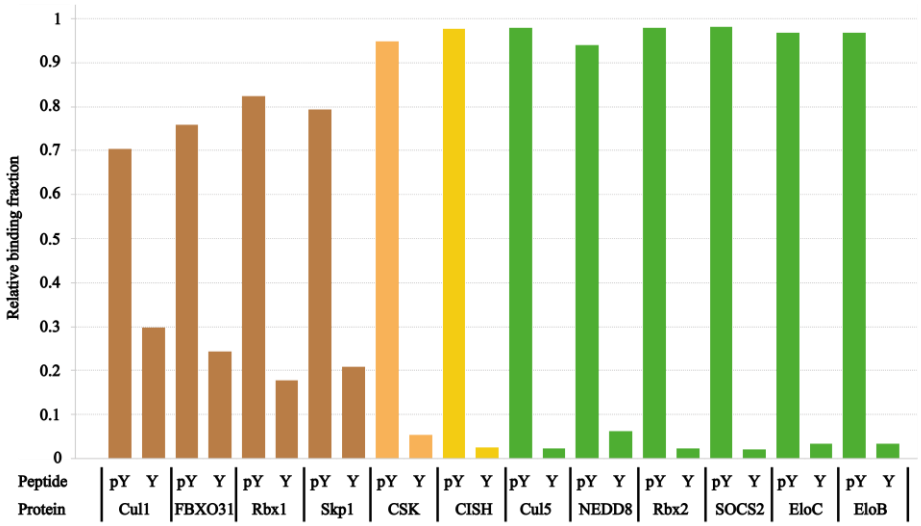

TABLE S1. Proteins specifically enriched by the phosphorylated GHR_pY595-modified beads.

Protein	UniProt ID	Comments
SOCS2	**O14508**	Suppressor of cytokine signaling 2. Substrate recognition domain of Cul5^{SOCS2} E3 ligase. Contains SH2 domain that recognizes substrate phospho-tyrosine residues.
EloB	**Q15370**	Transcription elongation factor B.
EloC	**Q15369**	Transcription elongation factor C. Complex of EloB and EloC (EloBC) serves as adaptor domain of Cul5^{SOCS2} E3 ligase.
Cul5	**Q93034**	Cullin 5. Scaffold domain of the Cul5^{SOCS2} E3 ligase.
Rbx2	**Q9UBF6**	RING-box protein 2. Contains RING-type zinc finger, recruits E2-conjugating enzyme.
NEDD8	**Q15843**	Neural precursor cell expressed developmentally down-regulated protein 8. Ubiquitin-like protein, can form covalent conjugate with Cullin that enhances the E3 ligase activity.
CISH	**Q9NSE2**	Cytokine-inducible SH2-containing protein. Component of SCF E3 ligase, can recognize phosphor-tyrosine.
Rbx1	**P62877**	RING-box protein 1. Contains RING-type zinc finger, recruits E2-conjugating enzyme.
CSK	**P41240**	C-Src kinase. Contains SH2 domain that can recognize phospho-tyrosine residues.
Cul1	**Q13616**	Cullin 1. Scaffold component of SCF E3 ligase.
FBXO31	**Q5XUX0**	F-box only protein. Substrate recognition component of SCF E3 ligase. Can recognize certain phosphorylated substrates.
Skp1	**P63208**	S-phase kinase-associated protein 1. Adaptor component of SCF E3 ligase.

FIGURE S2. Gel filtration UV traces for *A*, SOCS2-EloBC; *B*, Cul5$_{NTD}$; *C*, Cul5-Rbx2; *D*, SOCS2-EloBC-Cul5$_{NTD}$ and *E*, SOCS2-EloBC-Cul5-Rbx2. Proteins were purified using multi-step purification with the size-exclusion chromatography being the last step. Peak fractions corresponding to the appropriate proteins were pooled together. Purity and identity of each protein were confirmed using denaturing ESI-MS (data not shown) and SDS-PAGE.

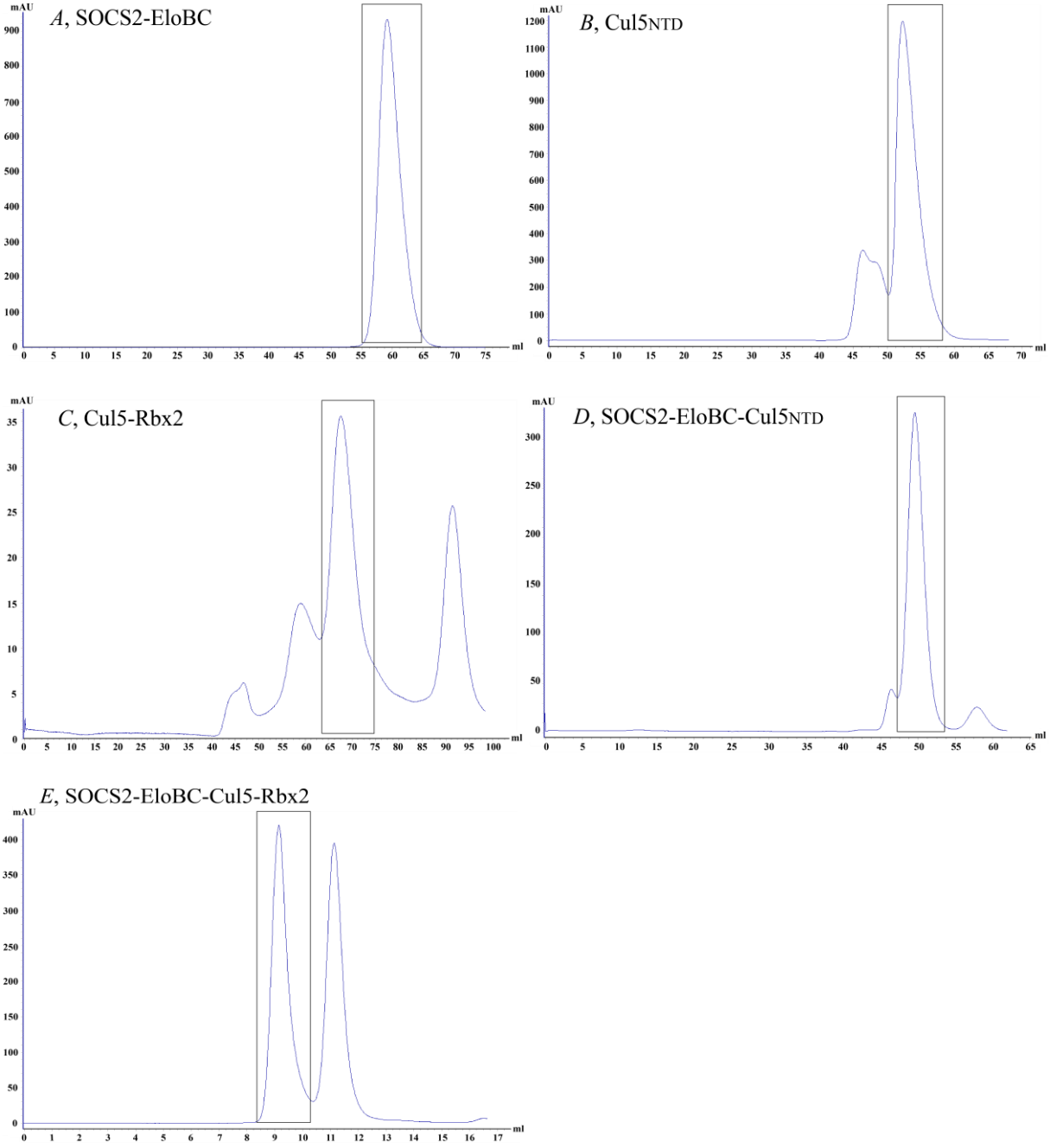

FIGURE S3. Native MS spectra for *A*, SOCS2-EloBC; *B*, $Cul5_{NTD}$ and *C*, Cul5-Rbx2.

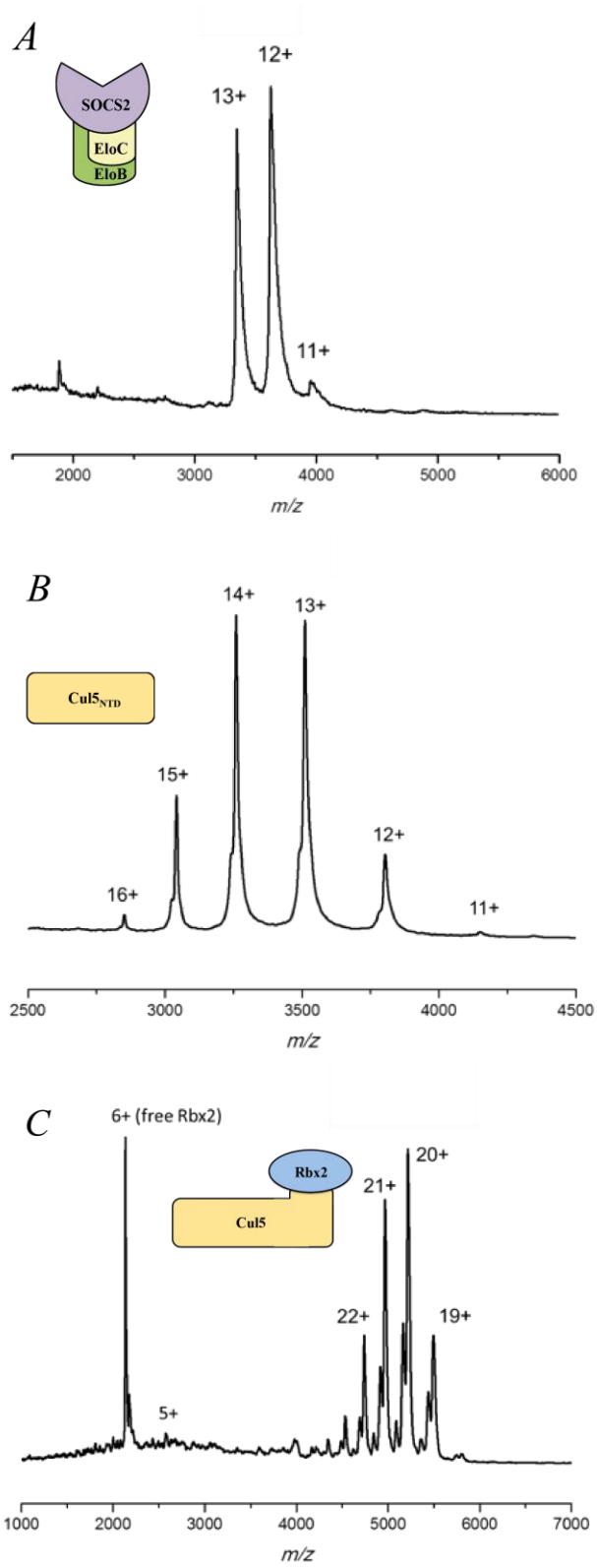

FIGURE S4. SDS-PAGE gel images of the neddylation reaction products. No neddylated product observed in negative control reaction (left). Right, neddylated Cul5-Rbx2-NEDD8.

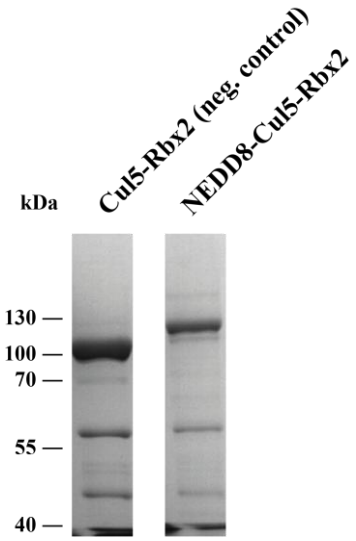

FIGURE S5. Native MS spectra comparison for *A*, Cul5-Rbx2-NEDD8; *B*, Cul5-Rbx2; *C*, SOCS2-EloBC-Cul5-Rbx2-NEDD8; *D*, SOCS2-EloBC-Cul5-Rbx2.

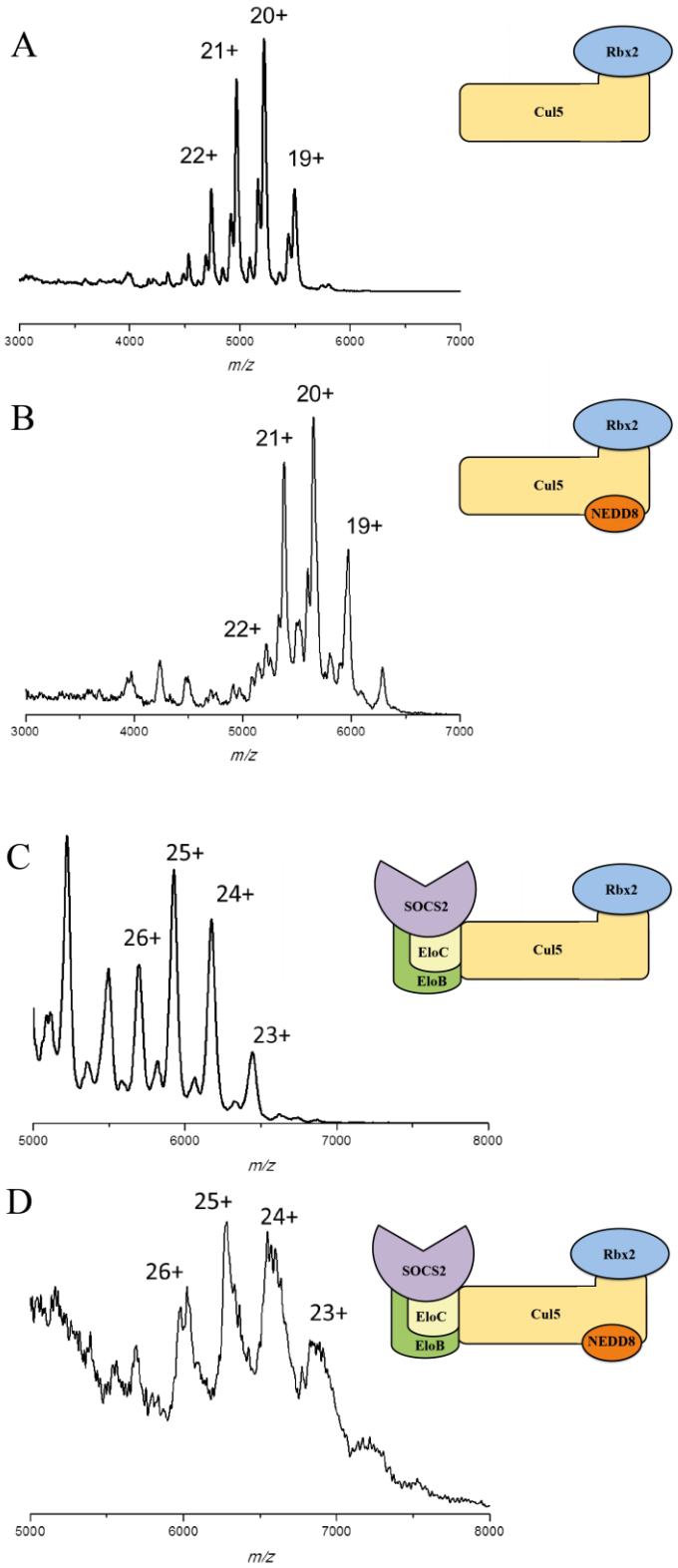

FIGURE S6. Structural models provide important insights into the assembly and architecture of $CRL5^{SOCS2}$. *A*, Cul5-Rbx1; *B*, NEDD8~Cul5-Rbx1 ("closed" model); *C*, NEDD8~Cul5-Rbx1 ("open" model); *D*, SOCS2-EloBC-Cul5-Rbx1; *E*, SOCS2-EloBC-NEDD8~Cul5-Rbx1 ("closed" model); *F*, SOCS2-EloBC-NEDD8~Cul5-Rbx1 ("open" model). The models were assembled using available crystal structures. Due to the lack of Rbx2 crystal structure, its closest homolog Rbx1 was used instead. These models were used for calculation of the theoretical CCS values.

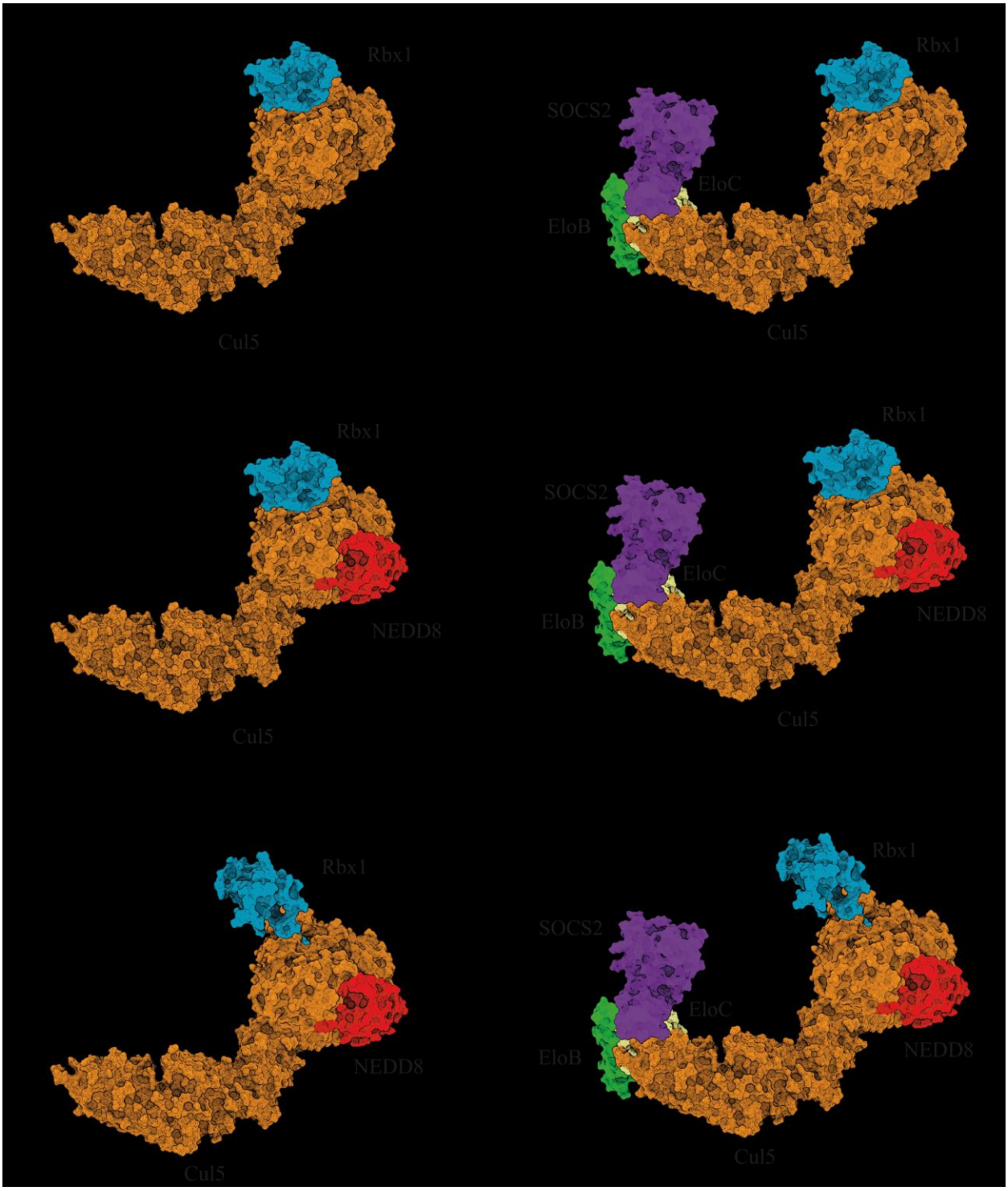
Rbx1
Cul5
Rbx1
SOCS2
EloC
EloB
Cul5
Rbx1
NEDD8
Cul5
Rbx1
SOCS2
EloC
EloB
NEDD8
Cul5
Rbx1
NEDD8
Cul5
Rbx1
SOCS2
EloC
EloB
NEDD8
Cul5